H_∞-Based Robust Torque Control of Harmonic Drive Systems

H. D. Taghirad
K. N. Toosi U. of Technology,
Dept. of Elec. Eng.,
P.O. Box 16315-1355,
Tehran, Iran 16314
e-mail: taghirad@eetd.kntu.ac.ir

P. R. Bélanger
Center for Intelligent Machines,
McGill University,
Montréal, PQ, H3A 2A7, Canada
e-mail: pbelanger@fgsr.mcgill.ca

In this paper, the torque control of a harmonic drive system for constrained-motion and free-motion applications is examined in detail. A nominal model for the system is obtained in each case from experimental frequency responses of the system, and the deviation of the system from the model is encapsulated by a multiplicative uncertainty. Robust torque controllers are designed using this information in an $\mathcal{H}_\infty$-framework, and implemented on two different setups. From time and frequency domain experiments, it is shown that the closed-loop system retains robust stability, while improving the tracking performance exceptionally well. To further improve the performance of the system for free-motion case, a feedforward friction-compensation algorithm is implemented in addition to the robust torque control. It is shown that friction-compensation will shrink the model uncertainty at low frequencies and hence, the performance of the closed-loop system will be improved at those frequencies. [DOI: 10.1115/1.1376714]

Keywords: Harmonic Drive, Torque Sensing, Torque Control, $\mathcal{H}_\infty$ Control, Robust Control, Nonlinear System, Empirical Linear Model, Multiplicative Uncertainty, Friction-Compensation

I Introduction

Robot manipulators require actuators with high torque capability at low velocities. On the contrary, electric motors provide their operating torque only at high velocities. Many electrically actuated robots, therefore, use a gear transmission to increase the torque and decrease the operating speed. Among gear transmissions, harmonic drives are high-ratio, compact, and lightweight mechanisms with almost no backlash (Fig. 1). These unique performance features of harmonic drives have captured the attention of designers.

In numerous robotic control techniques, such as feedback linearization, computed torque method, and some adaptive control schemes, the actuator torque is taken to be the control input [1,2]. The physical variable being manipulated in practice, however, is not torque but armature current in a DC motor, for instance. For harmonic drive systems the relation between output torque and input current possesses nonlinear dynamics, due to the flexibility, Coulomb friction, and structural damping of the harmonic drive [3]. The objective of this research is *to improve this input/output relation by torque feedback and to convert the system to a near-ideal torque source with a flat frequency response over a wide bandwidth*. There is a dichotomy of torque-control applications for a robotic manipulator using harmonic drives in its joints. First are applications where the robot is in contact with a stiff environment, and high torques at very low velocities are required at each joint. Simulation of this application at each joint can be studied by a constrained-motion experiment. The second class of applications occurs when the robot arms are moving freely, and the torque required at each joint is to compensate for gravity, friction, and link acceleration only. This problem can be simulated through a free-motion case, especially where the gear ratio is large enough for the motor inertia to dominate. In the free-motion case, the amount of torque required at each joint is very low but at much higher velocities. In this paper, the robust torque control of a joint for both constrained-motion, and free-motion application will be addressed in detail.

Throughout its short existence, the harmonic drive has enjoyed increasing international attention from designers as well as researchers. The Russians were perhaps the first who initiated substantial research on the dynamic behavior of harmonic drives [4]. More recently, Taghirad and Bélanger obtained simple and accurate models for friction, stiffness, and structural damping of harmonic drive systems and verified the performance of the simulated model with experiments in both constrained- and free-motion cases [3,5]. Tuttle performed an intensive effort to model the stiffness, positioning accuracy, gear tooth-meshing mechanism, and friction of the harmonic drive [6]. Kircanski and Goldenberg have also attempted to model the harmonic drive in detail [7]. Brigdes et al. [8], Kaneko et al. [9], Kazerooni [10], Hogan [11], Chapel and Su [12], Alter and Tsao [13], Kubo et al. [14], and Kang et al. [15], are representative of researchers who worked on the control of electric drive systems. Bridges used a very simple linear model for the system, with PD torque control. His results show some improvement in tracking error, but insufficient performance near resonant frequency. Kaneko also based his analysis on a simple model of the system, but included nonlinear stiffness in the system. He then applied a feedforward loop to adjust for nonlinear stiffness and then a pure gain torque feedback to shape the performance. Kazerooni considers a simple linear system for the harmonic drive, and used a sensitivity loop-shaping technique to design a linear controller for the system. Hogan proposed impedance control for robots with harmonic drive systems, to deal with the dynamic interaction induced in contact tasks, and Chapel applied $\mathcal{H}_\infty$ control design methods to the analysis and design of impedance control laws. Alter and Tsao have implemented $\mathcal{H}_\infty$ feedback control law on linear motor drives, while Kang et al., have used the same technique on robust tracking control of direct drive robot. Kubo examined friction-compensation on harmonic drives, and presented a stability analysis, and some experimental results of the improved performance of the system.

In this paper, a general framework to design torque controllers for harmonic drive system is developed and tested for constrained-motion and free-motion experiments [16,17]. A nominal model for the system is obtained from experimental frequency response estimates, and the deviation of the system from the model is encapsulated by a multiplicative uncertainty. Robust torque controllers are designed using this information in an $\mathcal{H}_\infty$-framework, and implemented on two different setups. From time and frequency domain experiments, it is shown that the closed-loop system maintains robust stability and improves the

Contributed by the Dynamic Systems and Control Division for publication in the JOURNAL OF DYNAMIC SYSTEMS, MEASUREMENT, AND CONTROL. Manuscript received by the Dynamic Systems and Control Division November 9, 1998. Associate Editor: P. Voulgaris.

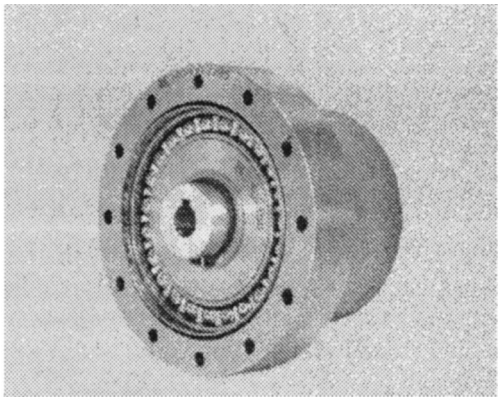

Fig. 1 Harmonic drive transmission

tracking performance exceptionally well. To further improve the performance of the system for free-motion application, a model-based, friction-compensation algorithm is implemented in addition to the robust torque control. It is shown that friction-compensation shrinks the model uncertainty at low frequencies and hence, the performance of the closed-loop system will be improved at those frequencies [17].

II Experimental Setup

Two harmonic drive testing stations were used to monitor the behavior of two different harmonic drives. A picture of those setups is illustrated in Fig. 2, in which the harmonic drive is driven by a DC motor, and a load inertia is used to simulate the robot arm for free motion. Also a positive locking system is designed such that the output load can be locked to the ground for restrained motion experiments. In the first setup [18], a brushed DC motor from Electro-Craft, model 586-501-113 is used. Its weight is 1.36 Kg, with maximum rated torque of 0.15 Nm, and torque constant of 0.0543 Nm/amp. The servo amplifier is a 100 Watts Electro-Craft power amp model Max-100-115. The harmonic drive in this setup is from RHS series of HD systems model RHS-20-100-CC-SP, with gear ratio of 100:1, and rated torque of 40 Nm. In the second setup [19], the DC motor is a brushless Kollmorgen Inland motor, model RBE-01503-A00. Its weight is 475 gr, with maximum rated torque of 5.6 Nm, and torque constant of 0.1815 Nm/amp. The servo amplifier is a FAST Drive Kollmorgen, model FD 100/5E1. The harmonic drive is from CFS series of HD Systems, Inc. with gear ratio 160:1, and rated peak torque of 178 Nm.

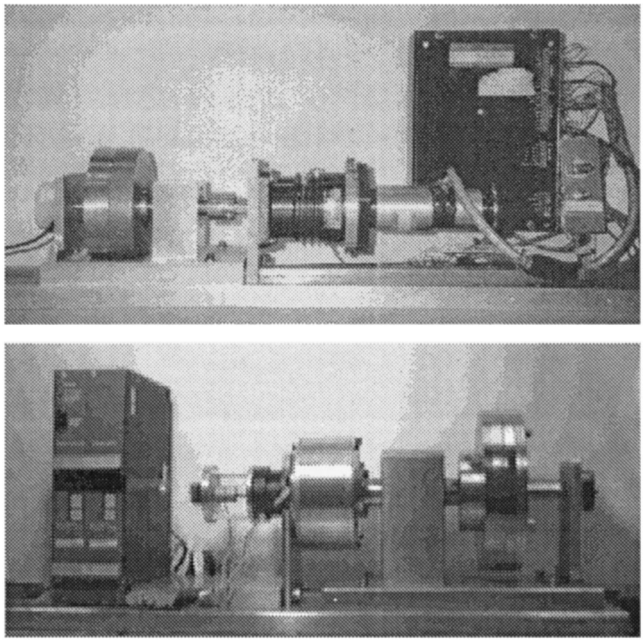

Fig. 2 A picture of the experimental setups for the two harmonic drives

Each setup is equipped with a tachometer to measure the motor velocity, and an encoder on the load side to measure the output position. The output torque is measured by a Wheatstone bridge of strain gauges mounted directly on the flexspline (detailed information on built-in torque sensor for harmonic drive system can be found in [20]). The current applied to the DC motor is measured from the servo amplifier output. These signals were processed by several data acquisition boards and monitored by a C-30 Challenger processor executing compiled computer C codes. Moreover, Siglab [21], a commercial DSP hardware linked to Matlab, is used for frequency response analysis. This hardware is capable of generating sine-sweep, random, and chirp function inputs to the system, and analyze the output and produce online frequency response estimates of the system.

III System Model and its Uncertainty

A complete model of the system was derived in [5]. To capture the system dynamics accurately, it is necessary to consider nonlinear models for friction and structural damping. However, for the purpose of control, a linear model for the system will be used for the synthesis. An empirical method to find this nominal model is to perform a series of experimental frequency response on the system, with different input amplitudes, and to find the best fit through them. By this method, not only the empirical nominal model of the system (without need of any linearization) will be determined, but also variations in the frequency response of the system, due to the nonlinearities, will be encapsulated with an uncertainty representation. Using Siglab-generated sine-sweep and random inputs with different amplitudes on each experimental setup, a set of frequency response estimates for the system is generated. A detailed description of the Siglab hardware, and the verification of frequency response estimate techniques is given in [22]. Applying an iterative Gauss-Newton routine on one of the frequency response estimates, a transfer function is obtained which minimizes the weighted least-squares error between the experimental frequency response and the model.[1] We call this transfer function the ''Nominal Model'' of the system (illustrated in Figs. 3 and 4). Moreover, the variation of each frequency response estimate from the nominal model can be encapsulated by a multiplicative uncertainty. Assuming that the nominal plant transfer function is $\mathbf{P}_0(s)$, define $\mathcal{P}$ as the family of possible models of the system which includes all the experimental frequency response estimates, and the nominal model of the system, by multiplicative uncertainty we consider:

$$\forall \mathbf{P}(s) \in \mathcal{P}, \quad \mathbf{P}(s) = (\mathbf{1} + \boldsymbol{\Delta}(s)\mathbf{W}(s))\mathbf{P}_0(s) \tag{1}$$

Here $\mathbf{W}(s)$ is a fixed transfer function, called the *uncertainty weighting function* and $\boldsymbol{\Delta}$ is a memoryless operator of induced norm less than unity [23]. Note that in this representation $\boldsymbol{\Delta}(s)\mathbf{W}(s)$ gives the normalized system variation away from 1 at each frequency:

$$\frac{\mathbf{P}(j\omega)}{\mathbf{P}_0(j\omega)} - 1 = \boldsymbol{\Delta}(j\omega)\mathbf{W}(j\omega) \tag{2}$$

Hence, since $|\boldsymbol{\Delta}| \leq 1$, then

[1] Function *invfreqs* in Matlab.

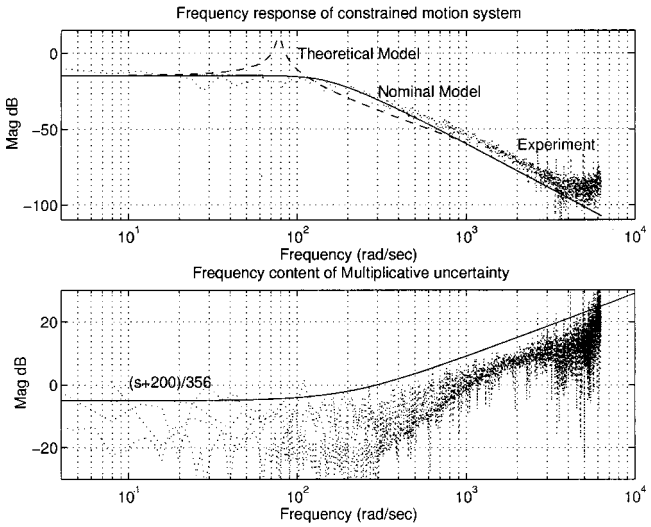

Fig. 3 Frequency response of the system under constrained-motion, theoretical and nominal models, and multiplicative uncertainty

$$\left|\frac{\mathbf{P}(j\omega)}{\mathbf{P}_0(j\omega)}-1\right|\leq|\mathbf{W}(j\omega)|,\quad \forall\omega \tag{3}$$

By plotting the system variations $|\mathbf{P}(j\omega)/\mathbf{P}_0(j\omega)-1|$, for all experimental frequency response estimates of the system $\mathbf{P}(j\omega)$, and estimating an upper bound to those variation as a transfer function, the multiplicative uncertainty weighting function $\mathbf{W}(s)$ will be obtained (as illustrated in Figs. 3 and 4).

As another method to obtain a linear model for the system, the nonlinear equation of motion of the system (given in [22]) can be linearized in a neighborhood of origin of the state space, which can be shown to be an equilibrium point for the system. The linear model derived by this means is called a ''Theoretical Model'' and illustrated in Fig. 3. The main difference between the nominal model and the theoretical model is at the resonant frequency, which is mainly due to ignoring the nonlinear friction terms in the linearization process of the theoretical model. For the purpose of control synthesis, the nominal model of the system gives better representation of the true dynamics, and thus is used for controller design. Note that by this method an effective way to find the closest linear model for a nonlinear system is proposed, and the deviation of the nonlinear system and linear model is encapsulated in model uncertainty. For a harmonic drive system the uncertainty measure at low frequencies (as illustrated in Figs. 3 and 4), is relatively small and about -5 db, which suggest the possibility of robustly controlling the system to perform within this bandwidth.

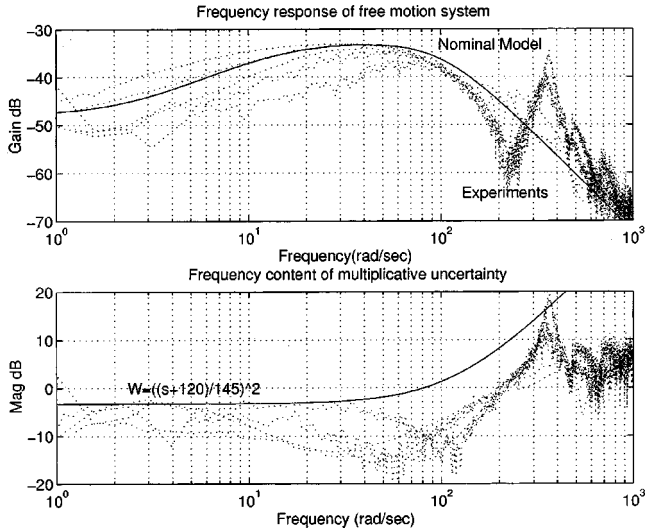

Fig. 4 Frequency response of the free-motion system, nominal model, and multiplicative uncertainty

A. System Under Constrained-Motion. The methodology elaborated in Section III is applied for two setups to obtain their nominal model and uncertainty. Since the results are similar, here we report only the results of the first experimental setup, while the details of the other can be found in [18]. Figure 3 illustrates the empirical frequency responses of the first setup under constrained-motion, its nominal model, and its uncertainty. The nominal model for the first setup is found to be a good fit to a third-order stable and minimum phase transfer function as follows:

$$\frac{\text{Torque}}{\text{Ref Voltage}}=\frac{1.0755\times10^6}{s^3+472.7s^2+7.33\times10^4s+5.89\times10^6} \tag{4}$$

which has three stable poles at -289.83, and $-91.44\pm109.48j$, and a DC-gain of -14.8 dB. Using Eq. (3) the system variations for four typical frequency response estimates is illustrated in Fig. 3, and the uncertainty weighting function is approximated by $\mathbf{W}(s)=(s+200)/356$.

B. System Under Free-Motion. Similar to the constrained-motion case, an empirical nominal model for the system is derived using experimental frequency response on the system for free-motion experiments. Figure 4 illustrates the empirical frequency responses of the system under free-motion, its nominal model, and its uncertainty bound. The nominal model for the system is found to be a third-order stable and minimum phase transfer function as follows:

$$\frac{\text{Torque}}{\text{Ref Voltage}}=\frac{243.16(s+2.415)}{s^3+171.19s^2+1.24\times10^4s+1.47\times10^5} \tag{5}$$

which has three stable poles at -14.465, and $-78.363\pm63.288j$, and a DC-gain of -48 dB. The uncertainty weighting function is approximated by a second-order system as: $\mathbf{W}(s)=((s+120)/145)^2$. Note that the lower DC-gain in free-motion system is due to smaller torque outputs in free-motion experiments compared to the constrained-motion case. Also, the system variations in free-motion are larger than that in the constrained-motion, since the nonlinear friction plays a more important role for low-frequency, free-motion experiments. These two factors make the control of free-motion case harder than that in the constrained-motion case. Moreover, the resonance/anti-resonance feature of the empirical frequency response of the free-motion system, observed at frequencies about 200 and 400 (rad/s) of Fig. 4, represents the typical higher mode vibration of the flexspline. The nominal model of the system is not representing the higher mode vibration of the system, and these unmodelled dynamics are encapsulated by an increasing uncertainty at high frequencies.

IV Robust Torque Controller Synthesis

Figure 5 illustrates the block diagram of the setup using multiplicative uncertainty representation, in which $\mathbf{P}_0$ is the nominal model of the system, $\mathbf{W}$ is the uncertainty weighting function, $\mathbf{\Delta}$ is a memoryless operator of induced norm less than unity, which represents the normalized variation of the true system from the model, and $\mathbf{C}$ is the controller. The control objective can be defined as *robustly stabilizing the system, while maintaining good disturbance attenuation and small tracking error, despite the actuator saturation*. More specifically, referring to Fig. 5, we would like to design a controller to trade-off minimizing the norm of the transfer function from reference input y_d to the tracking error e (tracking performance), the transfer function from the disturbance d to the output y (disturbance attenuation), the transfer function

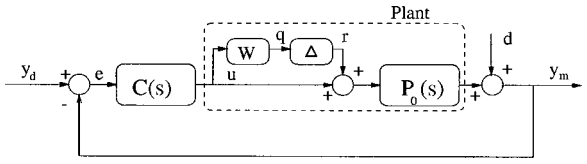

Fig. 5 Block diagram of the system considering multiplicative uncertainty for the plant

from r to q (robust stability), and the transfer function from reference input y_d to the plant input u (actuator limit). This objective is well-suited to the general $\mathcal{H}_\infty$ problem.

Figure 6 illustrates the block diagram of the system configured for the $\mathcal{H}_\infty$ framework. It can be shown that tracking and disturbance attenuation objectives can be expressed as sensitivity **S** minimization [24]. For multiplicative uncertainty robust stability is guaranteed if the complementary sensitivity **T** has a norm less than unity (Small Gain Theorem, Zames [25]). **T** can be shown to be the transfer function from reference input y_d to the output y. Weighting functions $\mathbf{W}_s$ and $\mathbf{W}_u$ are also considered to normalize and assign frequency content of the performance objectives on sensitivity and motor current saturation respectively, and **W** is the multiplicative uncertainty weighting function. Now the augmented system has one input y_d, and three outputs z_1, z_2, and z_3, in which the transfer function from the input to the outputs corresponds to weighted complementary sensitivity, weighted sensitivity, and weighted actuator effort, respectively. The objectives now will be reduced to finding the controller $C(s)$ which minimizes the induced norm of the transfer matrix from input y_d to the output vector **z** or,

$$\text{Find } C(s) \text{ to minimize } \|\mathbf{T}_{y_d\mathbf{z}}\|_\infty \tag{6}$$

This problem is called a mixed-sensitivity problem in the literature, and has optimal and suboptimal solution algorithms. Doyle et al. [23], provided the suboptimal solution for this problem in 1989, in which $C(s)$ will be assigned such that $\|\mathbf{T}_{y_d\mathbf{z}}\|_\infty < 1$. The μ-synthesis toolbox of Matlab uses this algorithm iteratively to find the best suboptimal solution achievable [26].

Performance-weighting functions are selected considering the physical limitations of the system. The actuator saturation-weighting function is considered to be a constant, by which the maximum expected input amplitude never saturates the actuator. Its value is estimated to be 0.004 for the system under constrained-motion, and 0.002 for free-motion case.

The sensitivity weighting function for constrained-motion setup is assigned to be $\mathbf{W}_s(s) = (s+300)/(2(s+3))$. This weighting function indicates that at low frequencies, the closed-loop system should reject disturbance at the output by a factor of 50 to 1. Expressed differently steady-state tracking errors due to step input should be less than 2 percent or less. This performance requirement becomes less and less stringent at higher frequencies. For higher frequencies the closed-loop frequency response should degrade gracefully, always lying underneath the inverse of the weighting function $\mathbf{W}_s$. For free-motion the sensitivity weighting function is assigned to be $\mathbf{W}_s(s) = (s+280)/(5(s+2.8))$, where 5 percent steady-state tracking error for the closed-loop system is allowed for free-motion case. The different choice of sensitivity weighting function for free-motion and constrained-motion permit us to have similar bandwith characteristics for the closed-loop systems despite the lower torque output and signal–noise ratio observed in the free-motion case. For both cases, the best cut-off frequency for performance is maximized by an iterative method, provided the $\mathcal{H}_\infty$ solution to the problem exist.

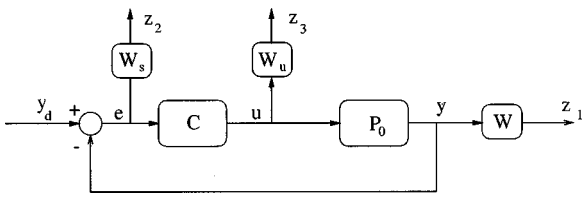

Fig. 6 Block diagram of system in $\mathcal{H}_\infty$ framework

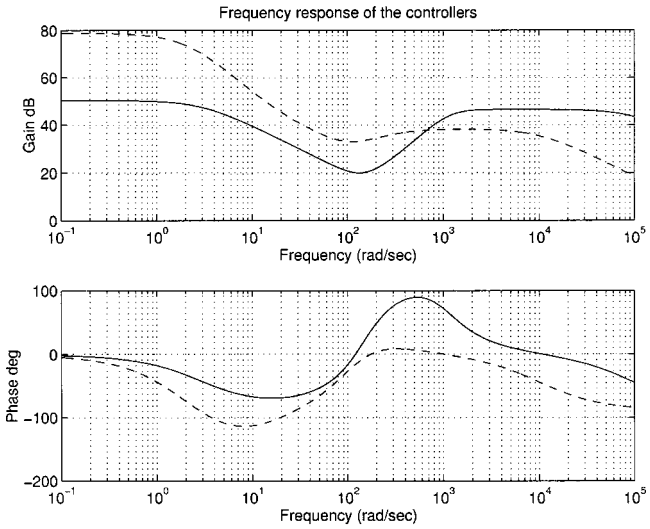

Fig. 7 The frequency response of the two designed controllers; solid: constrained-motion, dashed: free-motion

Two controllers were designed using μ-synthesis toolbox of Matlab. For constrained-motion case the controller transfer function is:

$$\mathbf{C}(s) = \frac{2.08\times 10^7 (s+289.8)(s+91.4\pm 109.5j)}{(s+3)(s+808.2\pm 776.04j)(s+9.8\times 10^4)} \tag{7}$$

with a DC-gain of 50.4 dB, while for free-motion case the controller is as follows with a DC-gain of 78.8 dB.

$$\mathbf{C}(s) = \frac{8.345\times 10^5 (s+14.5)(s+78.4\pm 63.3j)}{(s+1.83)(s+2.8)(s+273.23)(s+1.0\times 10^4)} \tag{8}$$

The controller zeros cancel the stable poles of the nominal plant, while the poles shape the closed-loop sensitivity function to lie underneath $\mathbf{W}_s$. Figure 7 illustrates the Bode plot of the two controllers, where for both controllers there is a wide anti-resonance profile around resonance frequency, to shape the complementary sensitivity function as flat as possible. Hence, it is not possible to obtain similar performance through a PID, or lead-lag controller. Furthermore, the free-motion controller has larger DC-gain to compensate for the comparatively lower measured torque signal.

V Closed-Loop Performance

To verify the controller performance, closed-loop experiments have been utilized. To implement the controllers in practice, bilinear discretization is performed with one kHz sampling frequency. The performance of the closed-loop system under constrained-motion and free-motion is evaluated in both frequency and time domain for two setups. However, because of the similarity in results, here only the experimental results of the first setup are presented.

A. System Under Constrained-Motion. The frequency domain performance of the closed-loop system is obtained from the closed-loop frequency response of the system and is illustrated in Fig. 8. For both setups the experimental sensitivity and complementary sensitivity functions are shown to be underneath the in-

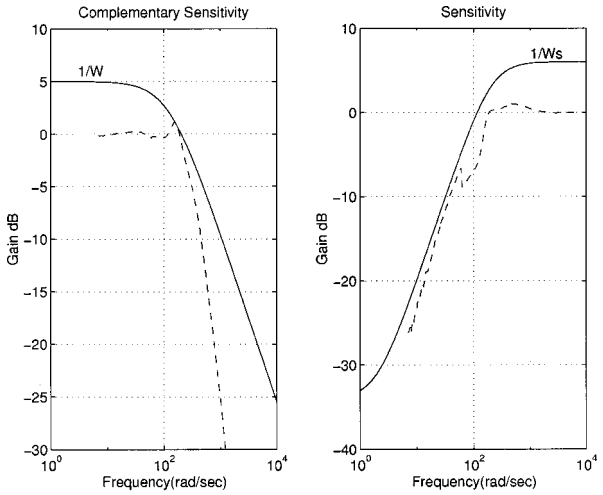

Fig. 8 Closed-loop frequency performance of the system under constrained-motion; solid: weighting functions inverse, dashed: experimental frequency responses

verse of $\mathbf{W}_s$, and $\mathbf{W}$, respectively. Also, the Nyquist plot for the loop-gain of the system is derived from the experimental sensitivity functions, and the phase margin is found to be 60 deg. These results are an experimental verification of the $\mathcal{H}_\infty$ design claim to preserve robust stability while shaping the performance as desired.

The time response of the closed-loop system to different reference input signals is illustrated in Fig. 9. The dotted lines are the measured output torque of the system, which is tracking the solid line, the reference command, very fast and accurately. Although our designed bandwidth is 3 rad/s, sinusoid inputs up to 10 Hz (62 rad/s) are shown to be well tracked. This is because of the conservativeness nature of the $\mathcal{H}_\infty$ synthesis. The step response is very fast with a steady-state error less than 2 percent as required. Tracking of the system to triangular signal is especially sharp at the edges, and the tracking to an arbitrary signal is shown to be very fast and well-behaved. Controller robust performance is experimentally verified for a large number of experiments reported in [22] in detail.

B. System Under Free-Motion. The frequency domain performance of the closed-loop system is obtained from the closed-loop frequency response of the system and is illustrated in Fig. 10. The experimental sensitivity and complementary sensitivity functions are shown to be underneath the inverse of $\mathbf{W}_s$, and $\mathbf{W}$, respectively. Also the Nyquist plot for the loop-gain of the system is derived from the experimental sensitivity functions, and the phase margin is found to be 80 deg.

The time response of the closed-loop system to different reference input signals is illustrated in Fig. 11. The dotted lines are the measured output torque of the system, which is tracking the solid line, the reference command. Although our designed bandwidth is about 2.8 rad/s, sinusoid inputs up to 10 Hz (62 rad/s) are shown to be relatively well tracked. The step response is very fast and tracking of the system to a triangular signal is especially sharp at the edges. Finally, tracking to an arbitrary signal is shown to be very fast and well-behaved.

The performance of the closed-loop system under free-motion case is not as good as that in constrained-motion, because in constrained-motion experiments the open-loop system has a higher DC-gain, lower uncertainty at low frequencies, and higher signal-to-noise ratio. Hence, wider bandwidth and better closed-loop performance are achievable as illustrated in Fig. 9. Controller robust performance is experimentally verified for a large number of experiments reported in [22] in detail.

Moreover, in free-motion case the choice and amplitude of the

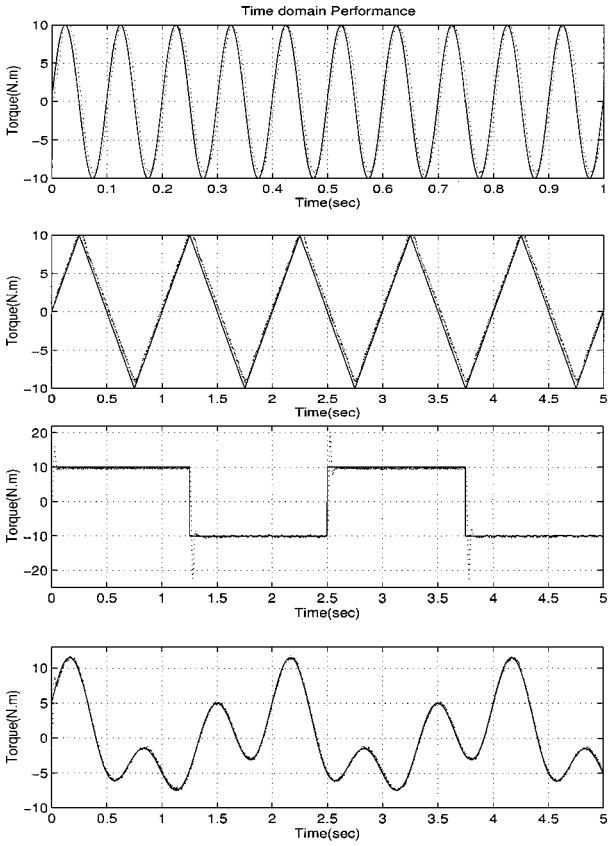

Fig. 9 Closed-loop performance of the system under constrained-motion; solid: reference command, dotted: experimental result

reference signal is limited, since the output torque of the system is proportional to the output acceleration of the load inertia plus some velocity dependent frictional losses at the output bearings. Hence, applying a step reference torque to the closed-loop system results in a constant acceleration for the system, which will be interrupted quickly as the motor reaches its maximum operating velocity. Therefore, in the free-motion closed-loop experiments

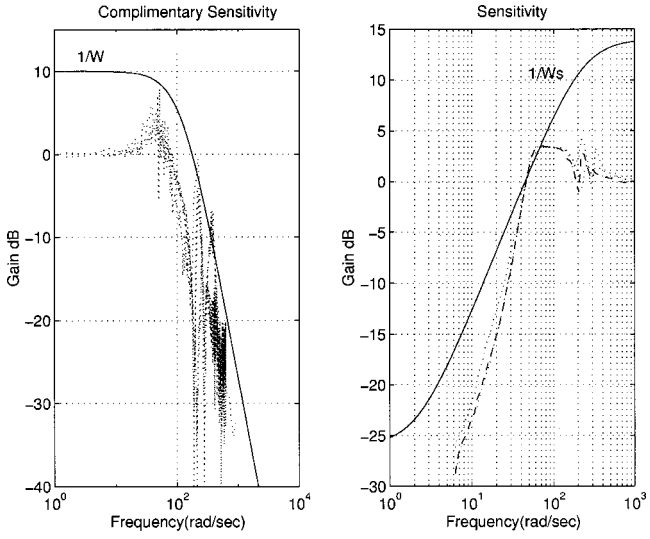

Fig. 10 Closed-loop frequency performance of system under free-motion; solid: weighting functions inverse, dashed and dotted: experimental frequency responses

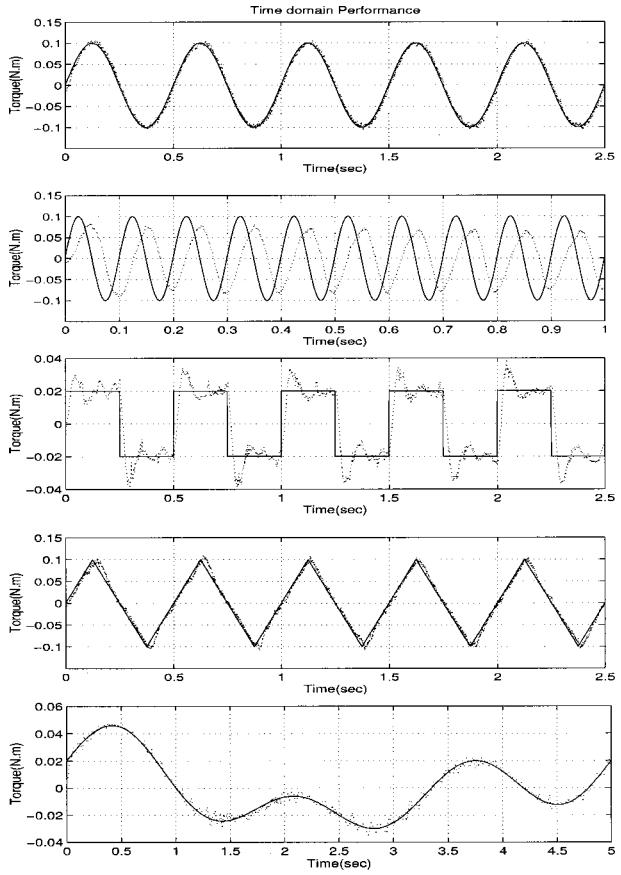

Fig. 11 Closed-loop performance of the system under free-motion; solid: reference command, dotted: experimental result

illustrated in Fig. 10 the amplitude of the reference torques is much lower than the constrained-motion case, and a squared-signal is used to assess the step response of the system.

VI Friction-Compensation

To improve the closed-loop performance of the system under free-motion, we applied a friction-compensation algorithm to the open-loop system. As is illustrated in Fig. 4, the frequency response of the system under free-motion possess significant variations at low frequencies. This is mainly caused by the nonlinear behavior of friction, which is more important at low frequencies. In [5], a complete model of harmonic drive friction is presented as Coulomb, viscous, and Stribeck friction. The friction parameters are carefully identified by experiments, and it is illustrated that the effect of Coulomb and Viscous friction is significant for free-motion experiments, while Stribeck friction is only important in constrained-motion experiment or in free-motion experiments at low velocities. Hence, in this study, we only compensate for Coulomb and viscous friction.

A. Friction-Compensation Algorithm. The identified friction in a harmonic drive system under study can be represented as:

$$T_{fric}(\dot{\theta}) = T_{v_n} u_{-1}(-\dot{\theta})\dot{\theta} + T_{v_p} u_{-1}(\dot{\theta})\dot{\theta} + T_{s_n} u_{-1}(-\dot{\theta})\text{sign}(\dot{\theta}) + T_{s_p} u_{-1}(\dot{\theta})\text{sign}(\dot{\theta}) \tag{9}$$

where

$$u_{-1}(x) = \begin{cases} 1 & \text{if } x > 0 \\ 0 & \text{if } x \leq 0 \end{cases} \tag{10}$$

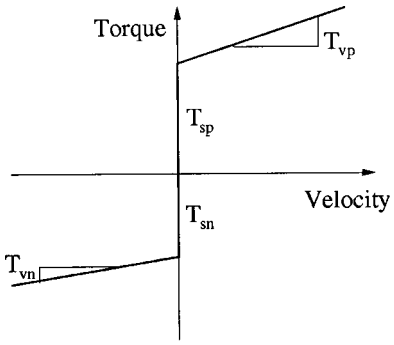

Fig. 12 Identified Coulomb and viscous friction curve for harmonic drive systems

$T_v n$ and T_{v_p} are the viscous friction coefficient depending on the direction of the velocity, and T_{s_n} and T_{s_p} are those of the Coulomb friction as illustrated in Fig. 12. The identified parameters for our harmonic drive are: $T_{v_n} = 3.5 \times 10^{-4}$, $T_{v_p} = 3.7 \times 10^{-4}$(N.m.s/rad), $T_{s_n} = 4.4 \times 10^{-2}$, and $T_{s_p} = 4.6 \times 10^{-2}$(N.m) [4].

The idea of friction-compensation is to estimate the friction torque at each instant from the measured velocity of the system, and increase the reference command to the servo-amp corresponding to the estimated friction. Ideally, estimated friction should be equal to the actual friction; however, the magnitude of the friction depends on the operating condition, and special care must be taken such that over-compensation does not occur, which introduces instability into the system. For our experimental setup, 90 percent of the estimated friction is compensated to avoid over-compensation as suggested by Kubo et al. [14]. Another practical issue in friction-compensation algorithm is the method of implementation of hard nonlinear Coulomb friction. The estimated friction will change signs as velocity crosses zero. In practice, however, the velocity measurement is sampled, and hence, zero velocity crossing may never coincide at the sampling instants. Moreover, the velocity signal is always contaminated with noise, and at low velocity several unrealistic zero crossings may appear. To avoid chattering problem for friction-compensation, there is a threshold velocity introduced in the literature [27–29] to smooth the hard nonlinearity of Coulomb friction. Including the *threshold velocity* $\dot{\theta}_t$, the final friction estimation function will be as follows [30]:

$$T_{fric} = \begin{cases} T_{v_p}\dot{\theta} + T_{s_p} & \dot{\theta} > \dot{\theta}_t \\ T_{v_p}\dot{\theta} + T_{s_p} & |\dot{\theta}| \leq \dot{\theta}_t \quad \& \quad V_{ref} > 0 \\ T_{v_n}\dot{\theta} - T_{s_n} & |\dot{\theta}| \leq \dot{\theta}_t \quad \& \quad V_{ref} < 0 \\ T_{v_n}\dot{\theta} - T_{s_n} & \dot{\theta} < -\dot{\theta}_t \end{cases} \tag{11}$$

in which V_{ref} is the reference voltage commanded to the servo-amp, and the threshold velocity is set to $\dot{\theta}_t = 1$(rad/s) for the experiments. Figure 13 illustrates the Block diagram of friction-compensation algorithm implemented on the setup. The estimated friction torque should be transformed to the command signal to the servo-amp and be added to the reference voltage. This has been done by dividing the friction torque estimate to the motor torque constant K_m(N.m/amp) and servo-amp gain G_{amp}(amp/volt) as illustrated in the diagram.

B. System Model and its Reduced Uncertainty. Similar to the free-motion case, an empirical nominal model for the system, including the friction-compensation, can be derived using experimental frequency response. Figure 14 illustrates the empirical frequency responses of the system with friction compensation, its

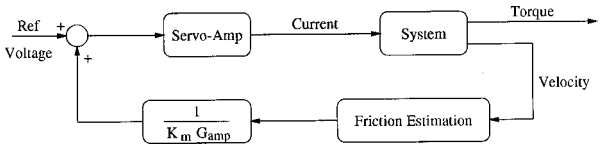

Fig. 13 Block diagram of the friction-compensation algorithm

nominal model, and its uncertainty weighting function. The effectiveness of friction-compensation to reduce the variation of the frequency response estimates at low frequencies is clearly shown by comparing Fig. 14 to Fig. 4. The friction compensated system behaves more linearly at low frequencies, and hence, the uncertainty of the system shrinks at low frequencies, from -3.3 dB to -10 dB. The uncertainty measure of the system is not only used in $\mathcal{H}_\infty$ synthesis to design the controller, but can be used also as a quantitative measure to show the effectiveness of the friction compensation algorithm.

The nominal model for the friction-compensated system is found to be a third-order stable and minimum phase transfer function as follows:

$$\frac{\text{Torque}}{\text{Ref Voltage}} = \frac{109.4(s+1.363)}{s^3+96.06s^2+5159s+2.71\times 10^4} \tag{12}$$

which has three stable poles at -5.868, and $-45.096\pm 50.953j$, and a DC-gain of -45.2 dB. The uncertainty weighting function is approximated by a second-order system as: $\mathbf{W}(s) = (s+120/213.4)^2$.

C. Robust Torque Control. Similar to the free-motion case, for the friction-compensated system a controller is designed using $\mathcal{H}_\infty$ framework. The sensitivity weighting function is assigned to $\mathbf{W}_s(s)=(s+530)/(5(s+5.3))$, which has a bandwidth of 5.3 (rad/s), as compared to 2.8 (rad/s) bandwidth in free-motion system is a significant improvement. Moreover, this weighting function assigns 5 percent steady-state tracking error similar to the free-motion system. This performance criteria can be strengthen to 2 percent in another trial, but with a reduced bandwith of 1.75 (rad/s). The actuator saturation-weighting function is considered to be 0.002, the same as what was assigned in free-motion case. The controllers were designed using μ-synthesis toolbox of Matlab by solving the mixed-sensitivity problem explained in Section IV. For friction-compensated system the controller transfer function is:

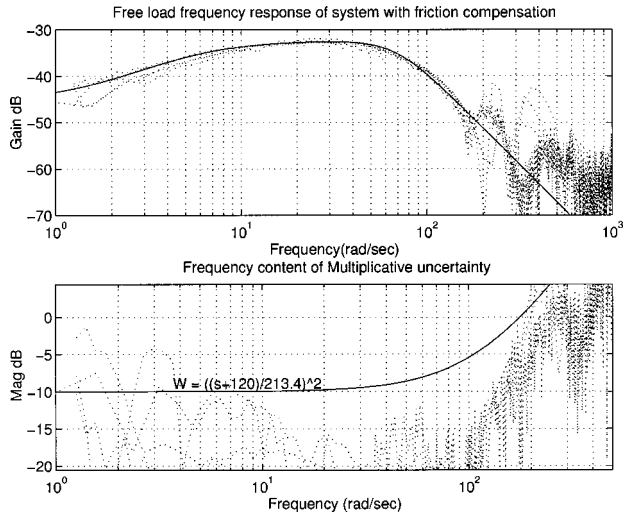

Fig. 14 Frequency response of the free-motion system with friction compensation, its nominal model, and multiplicative uncertainty

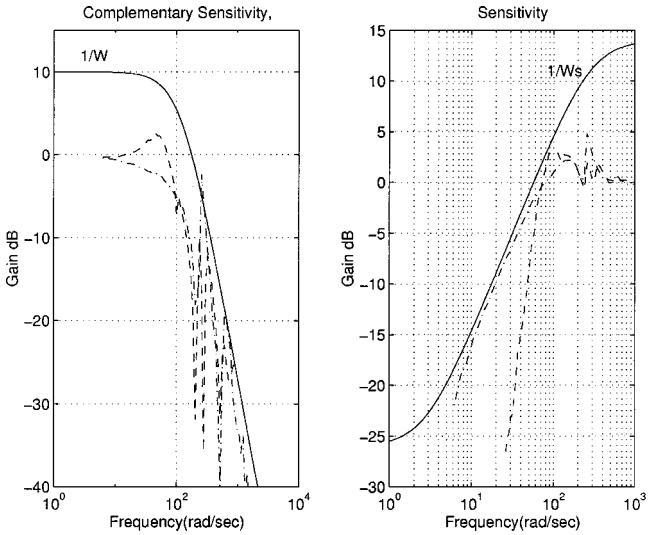

Fig. 15 Closed-loop frequency performance comparison of the system with and without friction-compensation; dashed: with friction-compensation, dash-dotted: without friction-compensation

$$\mathbf{C}(s) = \frac{3.30\times 10^6(s+5.8679)(s+45.10\pm 50.95j)}{(s+1.27)(s+5)(s+318.86)(s+1.06\times 10^4)} \tag{13}$$

with a DC-gain of 72 dB.

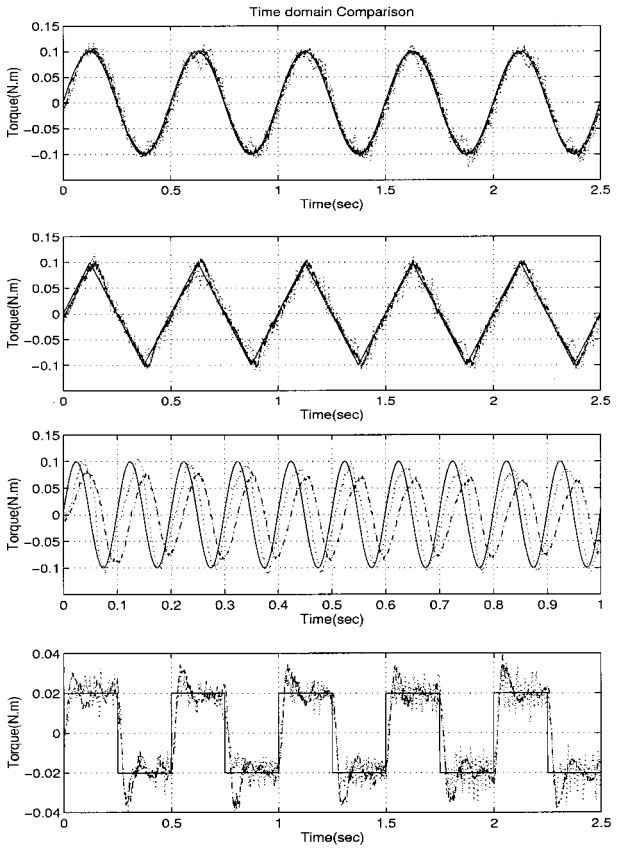

Fig. 16 Closed-loop time performance comparison of the system with and without friction-compensation; solid: reference command, dash-dotted: with friction-compensation, dotted: without friction-compensation

D. Closed-Loop Performance Comparison. To compare the performance of the closed-loop system with and without friction-compensation, frequency domain sensitivity and complementary sensitivity functions are shown in Fig. 15. The friction-compensated system have a smaller sensitivity function at low frequencies, compared to the system without friction-compensation; however, its complementary sensitivity function shows larger overshoot close to the resonance frequency. But that is well below the inverse of the uncertainty weighting function, and hence, the robust stability is not deteriorated. The performance comparison of the system in time domain is illustrated in Fig. 16. For low-frequency, sinusoid and triangular signal friction-compensation has improved the performance while for signals with high frequency content the performance is not improved, as illustrated for 10 Hz sinusoid and squared signals. Overall, for applications where tracking of slowly varying signals is intended, friction-compensation results in a better performance. However, if the tracking signal has fast variations friction-compensation doesn't contribute to better performance. The reason for that is, as illustrated in Fig. 14, friction-compensation will linearize the system only at low-frequencies, and moreover, a percentage of the system limited power is consumed for the friction-compensation, and less power is available for high frequency trackings. In our experimental setup depending on the output velocity 12–25 percent of the system power is utilized for friction-compensation algorithm.

VII Conclusions

In this paper, the torque control of harmonic drive systems under constrained-motion and free-motion is examined in detail. An effective method to obtain an empirical nominal model for the system from experimental frequency response estimates is proposed. By this means not only a linear model is nominated for the system, but also the deviation of the nonlinear system from the nominal model is encapsulated in a model uncertainty. This representation provides sufficient information to build a robust $\mathcal{H}_\infty$-based torque controller for the harmonic drive system. Solving the mixed-sensitivity problem for a tracking and disturbance attenuation objective, an $\mathcal{H}_\infty$ controller is designed accommodating the actuator saturation limits. An integral part of torque feedback is the Kalman filtered torque of the intelligent built-in torque sensor. Implementing the controllers for two different setups under two different operating conditions, the performance of the closed-loop system is evaluated experimentally. Exceptional performance results are obtained from the time and frequency response of the closed-loop system, especially for constrained-motion application. To further improve the performance of the system for the free-motion case, a model-based friction-compensation algorithm is implemented. It is shown that compensation of estimated Coulomb and viscous friction reduces the system frequency response variations, and hence, model uncertainty. The uncertainty measure is, therefore, not only used for control synthesis, but also as a quantitative indicator of the effectiveness of the friction-compensation algorithm. Finally, by comparison of the frequency and time domain performance of the system with and without friction-compensation, it is concluded that friction-compensation improves the performance of the system at low frequencies.

References

[1] S. Nicosia and P. Tomei, 1988, ''On the feedback linearization of robots with elastic joints,'' *Proceeding of IEEE Conference on Decision and Control*, **1**, pp. 180–185.

[2] Spong, M. W., 1989, ''Adaptive control of flexible joint manipulators,'' Syst. Control Lett., **13**, No. 1, pp. 15–21.

[3] H. D. Taghirad and P. R. Belanger, 1996, ''An experimental study on modelling and identification of harmonic drive systems,'' *Proceeding of IEEE Conference on Decision and Control*, **4**, pp. 4725–30, Dec.

[4] Volkov, D. P., and Zubkov, Y. N., 1978, ''Vibration in a drive with harmonic gear transmission,'' Russian Engineering Journal, **58**, No. 1, pp. 17–21.

[5] Taghirad, H. D., and Belanger, P. R., 1998, ''Modelling and parameter identification of harmonic drive systems,'' ASME J. Dyn. Syst., Meas., Control, **120**, pp. 439–444.

[6] Tuttle, T. D., and Seering, W. P., 1996, ''A nonlinear model of a harmonic drive gear transmission,'' IEEE Trans. Rob. Autom., **12**, No. 3, pp. 368–374.

[7] N. Kircanski, A. Goldenberg, and S. Jia, 1993, ''An experimental study of nonlinear stiffness, hysteresis, and friction effects in robot joint with harmonic drives and torque sensors,'' *Proceedings of the Third International Symposium on Experimental Robotics*, **1**, pp. 147–154.

[8] M. M. Bridges, D. M. Dawson, and S. C. Martindale, 1993, ''Experimental study of flexible joint robots with harmonic drive gearing,'' *Proceedings of the IEEE Conference on Control Applications*, **2**, pp. 499–504.

[9] K. Kaneko, T. Murakami, K. Ohnishi, and K. Komoriya, 1994, ''Torque control with nonlinear compensation for harmonic drive DC motors,'' *IECON Proceedings*, **2**, pp. 1022–1027.

[10] Kazerooni, H., 1995, ''Dynamics and control of instrumented harmonic drives,'' ASME J. Dyn. Syst., Meas., Control, **117**, No. 1, pp. 15–19.

[11] N. Hogan, 1991, ''Impedance control of robots with harmonic drive system,'' *Proceeding of the American Control Conference*, **1**, pp. 398–402.

[12] J. D. Chapel, 1991, ''Attaining impedance control objectives using $\mathcal{H}_\infty$ design methods,'' *Proceeding of IEEE International Conference on Robotics and Automation*, **2**, pp. 1482–87.

[13] Alter, D. M., and Tsao, T. C., 1996, ''Control of linear motors for machine tool feed drives: Design and implementation of $\mathcal{H}_\infty$ optimal feedback control,'' ASME J. Dyn. Syst., Meas., Control, **118**, No. 4, pp. 649–656.

[14] T. Kubo, G. Anwar, and M. Tomizuka, 1986, ''Application of nonlinear friction compensation to robot arm control,'' *Proceeding of IEEE International Conference on Robotics and Automation*, **1**, pp. 722–727.

[15] Kang, B. S., Kim, S. H., Kwak, Y. W., and Smith, Craig S., 1999, ''Robust tracking control of a direct drive robot,'' ASME J. Dyn. Syst., Meas., Control, **121**, pp. 261–269.

[16] H. D. Taghirad, and P. R. Belanger, 1997, ''Intelligent torque sensing and robust torque control of harmonic drive under free-motion,'' *Proceeding of IEEE International Conference on Robotics and Automation*, **2**, pp. 1749–54, April.

[17] H. D. Taghirad, and P. R. Belanger, 1997, Robust torque control of harmonic drive under constrained motion. *Proceeding of IEEE International Conference on Robotics and Automation*, **1**, pp. 248–253, April.

[18] Taghirad, H. D., 1997, ''On the robust h_∞-based torque control of harmonic drive systems,'' Technical Report TRCIM-97-05, Center for Intelligent Machines, McGill University, Apr.

[19] Taghirad, H. D., Belanger, P. R., and Helmy, A., 1996, ''An experimental study on harmonic drive,'' *Technical Report Submitted to the International Submarine Engineering Ltd., Port Coquitlam, BC, Canada*.

[20] Taghirad, H. D., and Belanger, P. R., 1998, ''Torque ripple and misallignment torque compensation for the built-in torque sensor of harmonic drive system,'' IEEE Trans. Instrum. Meas., **47**, No. 1, pp. 309–315.

[21] Signal Analysis Group, 1994, *DSP Technology Inc. Siglab Version 1.0*. DSP Technology Inc., 48500 Kato Road, Fremont, CA 94538-7385.

[22] H. D. Taghirad, 1997, ''*Robust torque control of harmonic drive systems*,'' PhD thesis, McGill University, Mar.

[23] Doyle, J., Glover, K., Khargonekar, P. P., and Francis, B. A., 1989, ''State-space solution to standard $\mathcal{H}_\epsilon$ and $\mathcal{H}_\infty$ control problems,'' IEEE Trans. Autom. Control, **AC-34**, pp. 831–847.

[24] P. R. Belanger, 1995, ''*Control engineering, a modern approach, Chapter 8*,'' Saunders College Publishing, 6277 Sea Harbor Drive, Orlando, FL.

[25] Zames, G., 1996, ''On the input-output stability of time-varying nonlinear feedback systems,'' IEEE Trans. Autom. Control, **II**, pp. 228–238 (part I), and 465–576 (Part II).

[26] G. J. Balas, J. C. Doyle, K. Glover, A. Packard, and R. Smith, 1991, ''*μ-Analysis and Synthesis Toolbox*,'' The Math Works, Inc., P.O. Box 1337, Minneapolis, MN 55414-5377.

[27] Adams, J., and Payandeh, S., 1996, ''Methods for low-velocity friction compensation: theory and experimental study,'' J. Rob. Syst., **13**, pp. 391–404, June.

[28] Armstrong-Helouvry, B., Dupont, P., and de Wit, C. Canudas, 1994, ''A survey of models, analysis tools and compensation methods for control of machines with friction,'' Automatica, **30**, pp. 1083–1138.

[29] Karnopp, D., 1985, ''Computer simulation of stick-slip friction in mechanical dynamic systems,'' ASME J. Dyn. Syst., Meas., Control, **107**, pp. 100–103.

[30] H. D. Taghirad and P. R. Belanger, 1998, ''Robust friction compensator for harmonic drive system,'' *Proceedings of the IEEE International Conference on Control Application*, **1**, pp. 547–551, Sept.